Supporting Information

Enhancing thermoelectric performance in hierarchically structured BiCuSeO by increasing bond covalency and weakening carrier-phonon coupling

Guang-Kun Ren, [a, b] *Shan-Yu Wang,* [b] *Ying-Cai Zhu,* [c] *Kyle J. Ventura,* [d] *Xing Tan,* [a] *Wei Xu,* [c] *Yuan-Hua Lin,* [a]* *Jihui Yang,* [b]* *and Ce-Wen Nan.* [a]

[a] State Key Laboratory of New Ceramics and Fine Processing, Department of Materials Science and Engineering, Tsinghua University, Beijing, 100084, P. R. China

[b] Material Science and Engineering Department, University of Washington, Seattle, Washington, 98195, USA

[c] Beijing Synchrotron Radiation Facility, Institute of High Energy Physics, Chinese Academy of Sciences, Beijing, 100049, P. R. China

[d] Department of Chemical and Biomolecular Engineering, University of Florida, Gainesville, Florida, 32610, USA

The coordinates corresponding to different atomic cluster size

Table S1 The coordinates around Te as Te occupies the Se site in the BiCuSeO

Shell index	Added coordinate atoms	Number of added atoms	Bond distance(Å)
1	Cu	4	2.22
2	Bi	4	2.83
3	O	4	3.06
4	Se	4	3.45
5	Bi, Se	1, 4	3.71
6	Cu	8	4.11
7	Bi, O	1, 8	4.62
8	Se	4	4.89
9	Bi	4	5.00
10	Cu	4	5.37
11	Bi	4	5.46
12	O	4	5.60
13	Se	4	5.61
14	Bi	8	5.64
15	O	4	5.76

Other thermal properties

The thermal diffusivity (D) was measured by a laser flash method (LFA-457, Netzsch, Germany) under a continuous Ar flow, and the data is shown in Fig. S1(a).

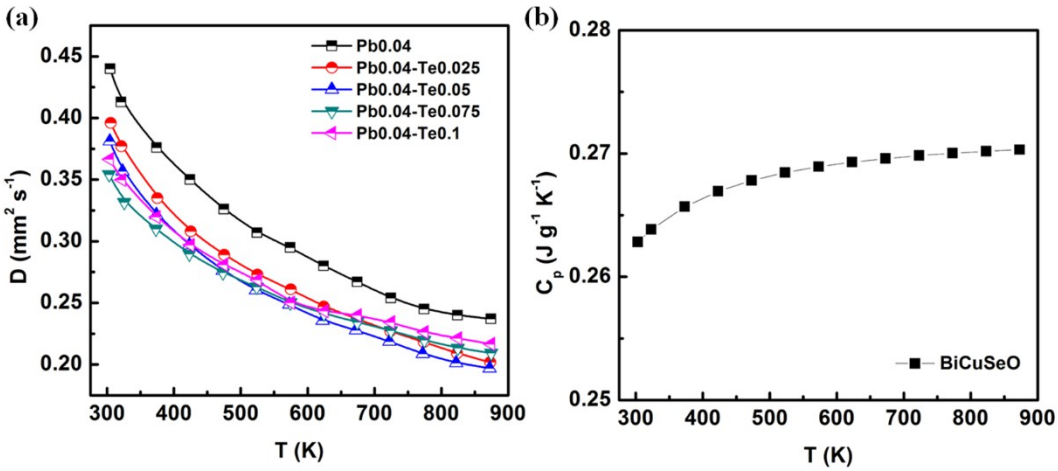

Fig. S1 (a) The measured thermal diffusion coefficient and (b) the specific thermal capacity as calculated by Debye model (similar to the Dulong–Petit law when $T > \Theta_D$).

As the thermal capacity (Fig. S1(b)) would not change a significant amount and C_p is the constant pressure

specific heat capacity which roughly equal to C_V (the constant volume specific heat capacity) in solids, we deduce it through the Debye model[1-3] (similar to the Dulong–Petit law when $T > \Theta_D$) and apply it for all samples, the uncertainty amongst different samples could be negligible. The formula for C_V is

$$C_V = \frac{9nR}{M}\left(\frac{T}{\Theta_D}\right)^3 \int_0^{\frac{\Theta_D}{T}} \frac{x^4 e^x}{(e^x - 1)^2} dx, \quad (1)$$

where R is the ideal gas constant, Θ_D the Debye temperature, n the atom number and M the molar mass of a primitive cell.

Lorenz number and effective mass

In order to analyze the transport properties of samples, we measured their carrier concentrations and mobilities by the Hall effect system, and based on the single band model and the electron-phonon interactionassumption, the Lorenz number (see graph Fig. S2) and the effective mass can be expressed as follows

$$S = \pm\frac{k_B}{e}\left(\frac{(r+5/2)F_{r+3/2}(\eta)}{(r+3/2)F_{r+1/2}(\eta)} - \eta\right), \quad (2)$$

$$n = \frac{1}{2\pi^2}\left(\frac{2m^* k_B T}{\mathsf{h}^2}\right)^{3/2} F_{1/2}(\eta), \quad (3)$$

$$F_i(\xi) = \int_0^{\infty} \frac{x^i dx}{1 + e^{x-\xi}}, \quad (4)$$

$$L = \left(\frac{k_B}{e}\right)^2 \left(\frac{(r+7/2)F_{r+5/2}(\eta)}{(r+3/2)F_{r+3/2}(\eta)} - \left[\frac{(r+5/2)F_{r+3/2}(\eta)}{(r+3/2)F_{r+1/2}(\eta)}\right]^2\right), \quad (5)$$

where e is the electronic charge, F_i is the Fermi integrals, and $\eta = E_F / k_B T$ is the reduce Fermi level, E_F is the electron Fermi level measured upward from the band edge. Meanwhile, the acoustic phonon scattering ($r = -1/2$) has been assumed as the main carrier scattering mechanism. The effective mass is calculated by Equations (2)-(4). The Lorenz number can be obtained by applying the calculated reduced Fermi energy η and scattering parameter r into Equation (5).[4]

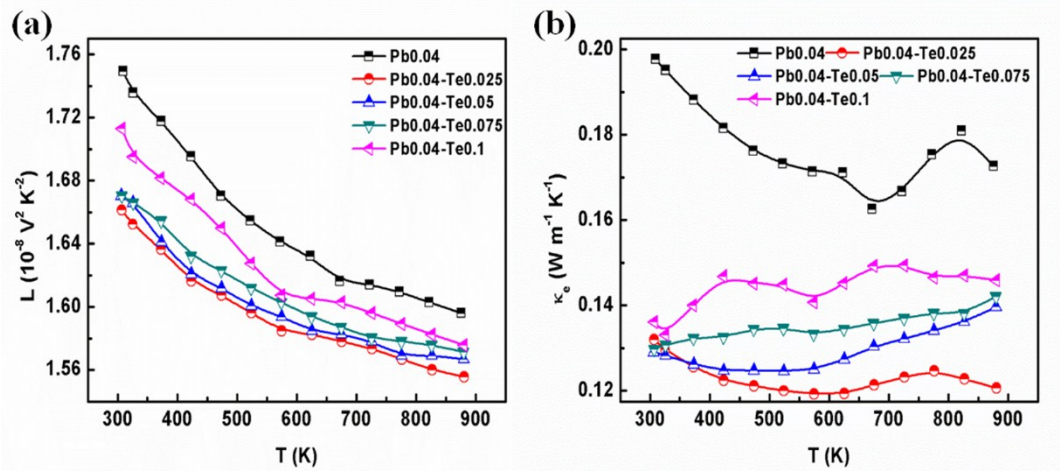

Fig. S2 (a) The calculated Lorenz number based on the single band model and the electron-phonon interaction assumption, (b) the electrical thermal conductivity (κ_e) calculated by the Wiedemann-Franz law.

Microstructure analysis by SEM

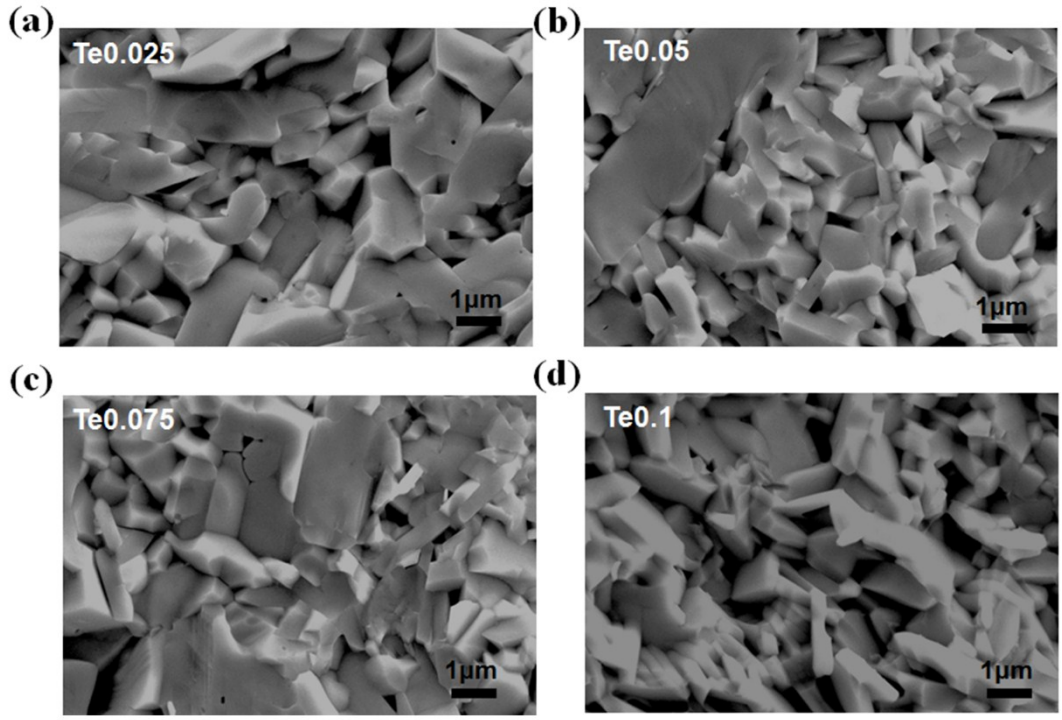

Fig. S3 The microstructures of $Bi_{0.96}Pb_{0.04}CuSe_{1-x}Te_xO$ (x = 0.025, 0.05, 0.075, and 0.1) samples.

Semi-quantitative calculation details of relaxation time approximation (RTA)

The Debye-Callaway model with relaxation time approximation (RTA) was utilized,[5-7] to calculated κ_L that can be expressed as

$$\kappa_L = \frac{k_B}{2\pi^2 \upsilon}\left(\frac{k_B}{\hbar}\right)^3 T^3 \int_0^{\frac{\Theta_D}{T}} \frac{\tau_c x^4 e^x}{(e^x - 1)^2} dx \ , \qquad (6)$$

where $x = \hbar\omega / k_B T$, ω the phonon frequency, τ_c the total relaxation time, $\hbar$ the Planck's constant, Θ_D the Debye temperature, and υ the mean sound velocity. The overall relaxation rate τ_c^{-1} can be determined by combining various scattering processes as given

$$\tau_c^{-1} = \tau_N^{-1} + \tau_b^{-1} + \tau_d^{-1} + \tau_U^{-1} , \qquad (7)$$

where τ_N, τ_b, τ_d, and τ_U are the relaxation times for the Normal processes, boundary scattering, defect scattering, and the Umklapp processes, respectively. Then we can represent the effects of Pb/Te dual point defects by modulating τ_d, and mesoscale and nanoscale effects by adjusting τ_b. The relaxation time of boundary scattering can be further written as

$$\tau_b^{-1} = \tau_{Mesoscale}^{-1} + \tau_{Nano}^{-1} , \qquad (8)$$

where $\tau_{Mesoscale}$ and τ_{Nano} are the relaxation times for mesoscale grains and nanostructures (including $Cu_7Te_{4-x}Se_x$ nanoinclusions and Cu_2Se_x nanodots), respectively. Contributions of different scattering mechanisms (τ_i) to κ_L can be estimated and are shown in Fig. 6(b). The BiCuSeO single crystal only show phonon-phonon interactions at $T > 300$ K, including the Normal and Umklapp processes, and κ_L clearly shows a T^{-1} dependence from 300 to 900 K. By contrast, the additions of mesoscale grains and nanostructures as well as point effects, lead to a gradual κ_L reduction with the increasing magnitude of these scattering mechanisms, and meanwhile the temperature dependence of κ_L will also deviate from the T^{-1} relation at lower temperatures. Furthermore, Fig. 6(b) also shows the calculated partial and total phonon density of states (PDOS) of BiCuSeO primarily focusing at the acoustic phonon range (< 60 cm^{-1}).[8] The heavy Bi contributes mainly to the acoustic modes, while lighter Se and O have only minor contributions. This indicates substitution or doping at the Bi site could significantly interrupt heat-transport acoustic phonons. Fig. 6(b) also qualitatively illustrates the three functional frequency ranges: mesoscale at low frequency range, nanoscale at mid-frequency range, and atomic scale at high frequency range. It is noted that all these mechanisms primarily scatter the acoustic phonons which dominate the heat transport, and the point defects could possibly scatter some low frequency optical phonons with moderate heat-conducting capability.[8] Our all-scale hierarchic structures, as demonstrated above, could largely block the transport of wide-frequency phonons and thus give rise to a low κ_L.

References

1. K. Berggold, Universität zu Köln, 2006.
2. M. Gu, C. Q. Sun, Z. Chen, T. A. Yeung, S. Li, C. Tan and V. Nosik, *Phys. Rev. B*, 2007, **75**, 125403.
3. V. Lazarev, A. Izotov, K. Gavrichev and O. Shebershneva, *Thermochimica acta*, 1995, **269**, 109-116.
4. J. L. Lan, Y. C. Liu, B. Zhan, Y. H. Lin, B. Zhang, X. Yuan, W. Zhang, W. Xu and C. W. Nan, *Adv. Mater.*, 2013, **25**, 5086-5090.
5. G.-K. Ren, S. Butt, K. J. Ventura, Y.-H. Lin and C.-W. Nan, *RSC Adv.*, 2015, **5**, 69878-69885.
6. J. Callaway, *Phys. Rev.*, 1959, **113**, 1046.
7. J. Callaway and H. C. von Baeyer, *Phys. Rev.*, 1960, **120**, 1149.
8. H. Shao, X. Tan, G. Q. Liu, J. Jiang and H. Jiang, *Sci. Reports*, 2016, **6**, 21035.